Optical study on the doping and temperature dependence of the anisotropic electronic structure in bilayered manganites: $La_{2-2x}Sr_{1+2x}Mn_2O_7$ ($0.3 \leqslant x \leqslant 0.5$)

T. Ishikawa* and K. Tobe
Department of Applied Physics, University of Tokyo, Tokyo 113-8656, Japan

T. Kimura†
Joint Research Center for Atom Technology (JRCAT), Tsukuba 305-0046, Japan

T. Katsufuji‡
Department of Applied Physics, University of Tokyo, Tokyo 113-8656, Japan

Y. Tokura
Department of Applied Physics, University of Tokyo, Tokyo 113-8656, Japan
and Joint Research Center for Atom Technology (JRCAT), Tsukuba 305-0046, Japan
(Received 12 April 2000)

The electronic structure of bilayered manganite ($La_{2-2x}Sr_{1+2x}Mn_2O_7$) has been investigated by optical measurements. In the paramagnetic phase, the in-plane and out-of-plane optical spectra show a doping dependence reflecting the change in the orbital character of conduction electrons. A drastic electronic structural change has been observed with the evolution of in-plane magnetic ordering irrespective of the ferromagnetic (e.g., $x=0.4$) or antiferromagnetic ($x=0.3$) interbilayer magnetic coupling. The optical conductivity spectra of the ferromagnetic state show a strongly incoherent feature, such as a minimal Drude component followed by a dominant broad peak centered around 0.4 eV. Anomalies in the phonon spectra are found in the antiferromagnetic state of the $x=0.45$ and 0.5 compounds, indicating a different structural change accompanied by the *A*-type antiferromagnetic (and perhaps x^2-y^2-type orbital) ordering. The relevant charge ordering and lattice distortion may be responsible for the nonmetallic nature of the *A*-type antiferromagnetic phase.

I. INTRODUCTION

Perovskite-type manganites, $R_{1-x}A_xMnO_3$ (*R* and *A* being the rare-earth and alkaline-earth ions, respectively), have been investigated extensively since the late rediscovery of colossal magnetoresistance (CMR) phenomena.[1–4] One of the essential ingredients in physics of CMR is the double exchange (DE) interaction,[5–7] which is the ferromagnetic interaction arising from the strong on-site (Hund's-rule) coupling (J_H) between the charge carriers (e_g-like state) and the local spins (t_{2g}-like state). However, the features not only of CMR but also of the ferromagnetic metallic (FM) state at low temperatures cannot fully be explained only by the DE model. Some additional or competing interactions/instabilities appear to be important as well, such as the Jahn-Teller (JT) interaction or the e_g orbital degree of freedom. Relevant anomalous features of the electronic structure have been found in optical spectra[8–13] and photoemission spectra.[14,15] Drastic temperature (*T*) dependence of the electronic structure has been observed and interpreted by various scenarios such as the magnetization-dependent J_H-split band,[8,16] change of effective coupling strength of JT polaron,[9,10,12,17,18] or other mechanisms.[19–21] However, even the assignment of the major optical conductivity peak (around 1 eV) is not settled because of the existence of the various mechanisms to be considered.

Thus further investigation is required for understanding of the mechanism of CMR in connection with electronic structural change. Among them, the bilayered-structure manganites, $La_{2-2x}Sr_{1+2x}Mn_2O_7$, may offer another unique opportunity to investigate the generic features of the CMR manganites. This bilayered compound with a tetragonal structure at room temperature is the two-dimensional (2D) analog of the pseudocubic perovskite-type manganites, in which the DE interaction essentially works only within the respective MnO_2 layers.[22–24] A preliminary study on the optical spectra of the $x=0.4$ compound has been reported in Ref. 25. In this context, we report the systematic doping dependence. The layered structure is expected to induce the effective magnetic field on the Mn e_g orbital as a pseudospin and hence partially lift the orbital degeneracy of e_g conduction electrons. The anisotropic interaction causes remarkable phenomena such as enhanced MR,[22] anomalous temperature dependence of the lattice constant,[26,27] and so on.

Figure 1 shows the *T* dependence of the dc resistivity at 0 T and the magnetization (*M*) at 0.5 T ($H \perp c$; *c* axis is perpendicular to the MnO_2 plane) for $La_{2-2x}Sr_{1+2x}Mn_2O_7$ crystals ($x=0.3$–0.5, *x* representing the nominal hole concentration) investigated in the present study. As for the $x=0.3$ and 0.4 compounds, a fully spin-polarized metallic (half-metallic) state is realized as the ground state, while the bilayer units are antiferromagneticaly (for $x=0.3$; A_f type) or ferromagneticaly (for $x=0.4$) coupled along the *c* axis, respectively (see Fig. 2). The in-plane ($I \perp c$) and *c*-axis ($I \| c$) resistivity of the metallic compounds both show sharp drop concurrently with the appearance of the spontaneous

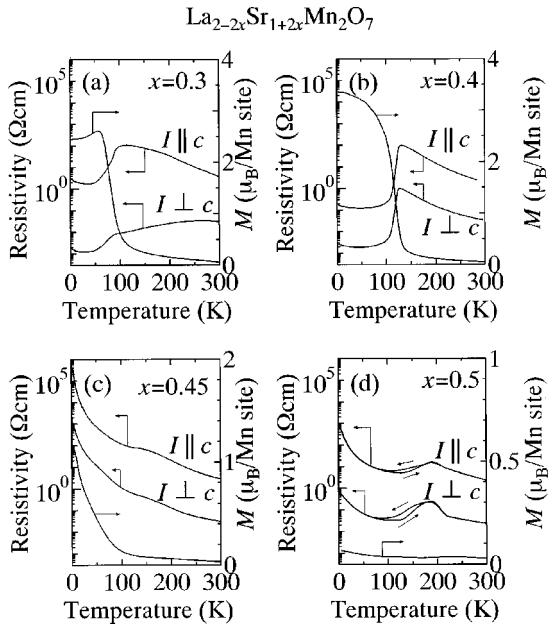

FIG. 1. Temperature dependence of the in-plane ($I\perp c$) and c-axis ($I\|c$) resistivity together with that of magnetization at 0.5 T ($H\perp c$) for $La_{2-2x}Sr_{1+2x}Mn_2O_7$ single crystals; (a) $x=0.3$, (b) 0.4, (c) 0.45, and (d) 0.5.

magnetization, which may correspond to the similar physics for the transition from paramagnetic insulating (PI) to FM phase in the pseudo cubic manganites. Metallic T dependence of the in-plane resistivity of the $x=0.3$ crystal even above the magnetic ordering temperature (T_c) may be attributed to the short-range ferromagnetic ordering in MnO_2 plane due to the strongly anisotropic exchange coupling.[23,28]

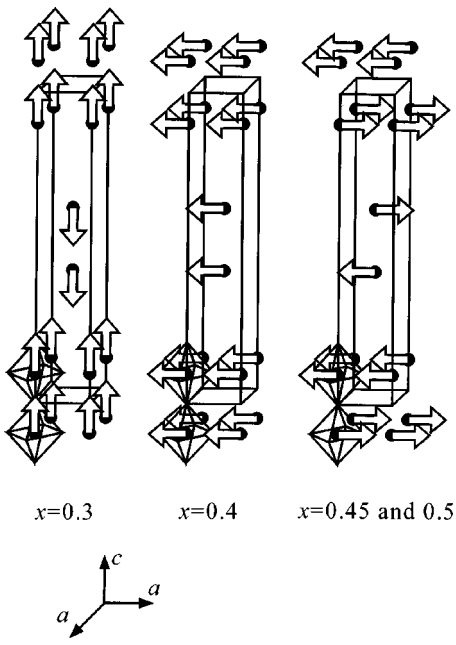

FIG. 2. Schematic magnetic structure in bilayer manganites (after Refs. 25, 26, and 28); A_F-type antiferromagnetic (AF) ordering (left), ferromagnetic ordering (middle), and A-type AF ordering (right). In each figure, arrows represent local spins and closed circles Mn ions.

A cusp feature of magnetization for $x=0.3$ corresponds to the rotation of the easy axis of Mn local moment which was observed in a recent neutron-scattering measurement.[29]

On the other hand, the low-T magnetization of the $x=0.45$ and 0.5 crystals, which are much smaller than those of $x=0.3$ and 0.4, arise from the spin canting between the MnO_2 planes in each bilayer unit. In other words, each crystal shows (canted) antiferromagnetic (AF) coupling along the c axis between fully spin-polarized ferromagnetic MnO_2 single layers.[30] Corresponding to the absence of the purely ferromagnetic order in the bilayer unit, the dc resistivity for each compound remains nonmetallic even in the magnetically ordered low-T phase. The ground state of the $x=0.45$ compound is canted AF phase and for the $x=0.5$ is A-type AF phase (see Fig. 2). It is worth noting that the difference between the FM phase and the A-type AF (or canted AF) phase is only the relative spin direction between the MnO_2 planes in each bilayer unit. Thus the magnetic structure of each single MnO_2 plane remains ferromagnetic irrespective of the x value in the ground state for these crystals ($0.3\leqslant x\leqslant 0.5$). We discuss in Secs. IV and VI the significant consequence of this apparently minor difference.

The outline of this paper is as follows. Section II describes the experimental procedures. We discuss the x dependence of orbital character on the basis of the optical spectra in Sec. III. Sections IV-VI are devoted to the discussion of T-dependent electronic structure; Sec. IV for the compounds ($x=0.3$ and 0.4) with the ferromagnetic metallic ground states, Sec. V for these metallic but anomalously incoherent charge dynamics showing up in low-energy conductivity spectra, and Sec. VI for the compounds ($x=0.45$ and 0.5) with the (canted) antiferromagnetic ground state. In Sec. VII, we argue the possible lattice distortion in A-type AF phase based on the phonon-spectral anomaly. We summarize the results and discussion in Sec. VIII.

II. EXPERIMENT

All the samples are single crystals grown by a floating-zone (FZ) method. Details were described in Refs. 22,23, and 31. Stoichiometric mixture of La_2O_3, $SrCO_3$, and Mn_3O_4 powder was calcined and sintered. Then, single crystals were grown by the FZ method at the feeding speed of 10-15 mm/h in O_2 gas flow. We confirmed the sample stoichiometry by inductively coupled plasma atomic emission spectroscopy. Atomic positions were determined by using the four-circle x-ray-diffraction measurement. Resistivity was measured by the conventional four-probe method and magnetization was measured by a commercial superconducting quantum interference device (SQUID) magnetometer.

We measured near-normal-incidence reflectivity spectra [$R(\omega)$] over a wide photon energy region (0.008-36 eV) at room temperature using the several light sources, polarizers, and detectors depending on the energy region. The polarized $R(\omega)$ spectra were measured on the ab (for $E\perp c$) and ac (for $E\|c$) faces of each single crystal with a typical size of $6\times 6\times 2$ mm^3. The ab face of the crystal was prepared by cleaving the crystal boule, while the ac face of the crystal was polished with alumina powder to a mirrorlike surface. To obtain the absolute value of reflectivity, we measured the reflection of a Au mirror as a reference below 1.5 eV. Above

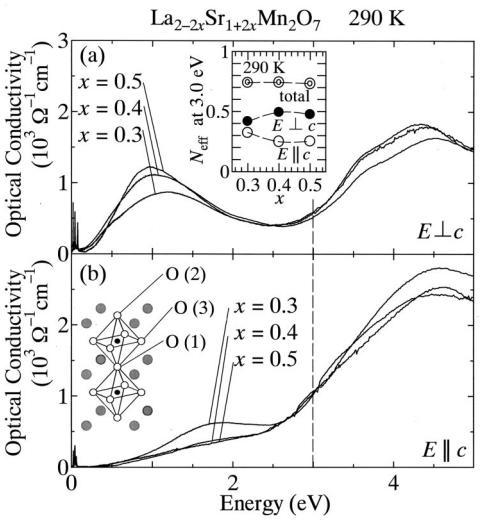

FIG. 3. The doping (x) dependence of the room-temperature (290 K) polarized optical conductivity spectra for the $La_{2-2x}Sr_{1+2x}Mn_2O_7$ single crystals; (a) in-plane ($E\perp c$) and (b) c-axis ($E\|c$) spectra. Inset to (a): the doping dependence of the effective number of electrons ($N_{\rm eff}$) at 3.0 eV. Closed, open, and double circles represent the $N_{\rm eff}$ values for (1) the in-plane spectra, (2) the c-axis spectra, and the sum of (1) and (2), respectively. Inset to (b): Schematic repeated cell of the bilayer manganite.

1.5 eV, where the $R(\omega)$ of Au is less than 98%, we directly detected the incident light by changing the light path. For the higher-energy (>6 eV) measurements, the synchrotron radiation at INS-SOR, Institute for Solid State Physics, University of Tokyo, was utilized as a polarized light source.

The temperature dependence of the polarized $R(\omega)$ spectra was measured by setting the sample and the reference mirror in a He gas-exchange-type cryostat. Above 4 eV, we were not able to detect a significant T-dependent change of spectra beyond the experimental error and use the room-temperature data above 6 eV to perform the Kramers-Kronig transformation. For the analysis, we assumed the constant reflectivity or Hagen-Rubens relation below 0.01 eV and ω^{-4} extrapolation above 36 eV. Variation of the extrapolation procedures was confirmed to cause negligible difference for the calculated conductivity spectra above 0.02 eV.

III. CHANGE OF THE ORBITAL CHARACTER WITH HOLE DOPING

Figures 3 (a) and (b) show the x dependence of the in-plane ($E\perp c$) and c-axis ($E\|c$) optical conductivity spectra at 290 K, which were obtained by Kramers-Kronig analysis of the polarized reflectivity data. At this temperature, all the samples are in the paramagnetic (PM) phase, thus we can compare the spectra without considering the difference of magnetic structure. Spiky structures in the far-infrared region ($\hbar\omega<0.07$ eV) are due to optical-phonon modes. T dependence of these phonon structures is discussed in Sec. VII in detail. The both in-plane and c-axis spectra show a peak at 4 eV. These peaks can be assigned to the charge-transfer (CT)-type transition between the O $2p$ and Mn $3d$ down-spin states.[32,33] The spectra below 3 eV, which show a clear anisotropic feature, are dominated by the intra- and interband transitions of the O $2p$ and Mn e_g hybridized states. The in-plane conductivity spectra [Fig. 3(a)] show a broad peak around 1 eV, forming a pseudogap (≈ 0.2 eV) structure.

This 1-eV peak may correspond to the intersite d-d transition between Mn^{3+} and Mn^{4+} site as in the case of $La_{1/2}Sr_{3/2}MnO_4$ (Refs. 34 and 35) which shows charge ordering at low T. However, a relatively large spectral weight of this peak implies strong hybridization of O $2p$ and Mn $3d$ states, i.e., CT-transition character. The mechanism that determines the peak energy as high as 1 eV remains unsettled at the present stage. The electron conrrelation effects or short-range charge/orbital ordering may be taken into account.[36] Anisotropic band dispersion should also be considered to account for the strong in-plane polarization of the 1-eV peak.

The spectral weight of this 1-eV peak apparently increases and the peak energy rather decreases with the doping level x. As for the c-axis spectra [Fig. 3(b)] in the energy region below 3 eV, a rather broad peak around 1.8 eV exists for the $x=0.3$ spectrum. To evaluate the doping dependence of the low-energy spectral weight, we have calculated the effective number of electrons ($N_{\rm eff}$), which is defined as

$$N_{\rm eff}(\omega)=\frac{2m}{\pi e^2 N}\int_0^{\omega}\sigma(\omega')\,d\omega'. \qquad (1)$$

Here, m represents the free-electron mass and N being the number of Mn atoms per unit volume. The inset to Fig. 3(a) shows that the value of $N_{\rm eff}$ at the cutoff energy 3 eV which corresponds to the onset energy of CT excitation to the t_{2g} orbital. The observed anisotropy of the absolute $N_{\rm eff}$ value for $E\perp c$ and $E\|c$ indicates that the kinetic energy of conduction electrons measured on this energy scale (3.0 eV) is suppressed for the c axis due to the layered structure. The c-axis $N_{\rm eff}$ value tends to decrease in accord with the increasing of x while the in-plane value increases. As shown in the inset to Fig. 3(a), the sum (double circles) of the $N_{\rm eff}$ values for $E\perp c$ and $E\|c$ shows a nearly x-independent value as if the spectral weight transfer occurred between the in-plane and the c-axis spectrum. This tendency signals the change of an electron occupation of the nearly degenerate e_g orbitals, x^2-y^2 vs $3z^2-r^2$. Recent diffraction measurement[37,38] shows that the increase of the doping decreases the lattice parameter of the c axis, especially the Mn-O(2) bond length [see the inset to Fig. 3(b)]. For example the ratio of the average Mn-O bond length along the c axis to the Mn-O(3) bond length [see the inset to Fig. 3(b)] is about 1.05 for $x=0.3$ and 1.02 for $x=0.4$ at room temperature.[37] This structural change can induce the change of the character of e_g electrons, from the $3z^2-r^2$ to the x^2-y^2 orbital as the doping increases. The change of the e_g orbital character can be closely related to the c-axis spectral weight, since the hybridization between Mn $3d$ x^2-y^2 and O $2p_z$ orbitals along the c axis (z axis) is zero by the symmetry, while the $3z^2-r^2$ electron can hop along the c axis through the $3d_{3z^2-r^2}$-p_z σ bonding state. In other words, the $3z^2-r^2$ character of e_g electrons produces the spectral weight for the c-axis spectrum. Therefore the relative change of the spectral weight with x is caused by the change of orbital character induced by the structural change. Such an idea of the orbital-character change with doping is also supported by the magnetic phase transition with x. For example, A-type AF phase in the highly

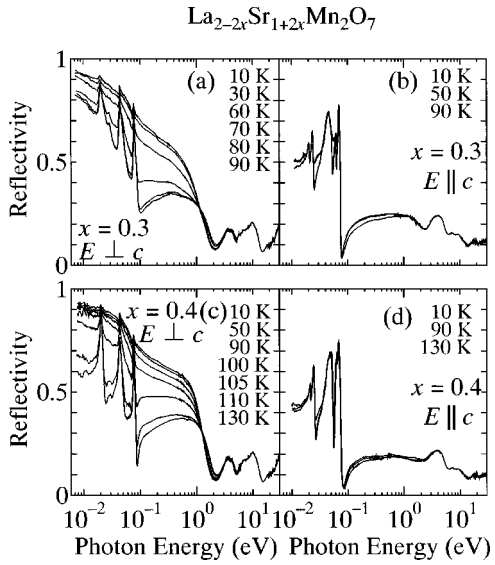

FIG. 4. Reflectivity spectra for $La_{2-2x}Sr_{1+2x}Mn_2O_7$ at the temperatures below the magnetic ordering temperature T_c. (a) In-plane reflectivity spectra for the $x=0.3$ crystal, (b) c-axis reflectivity spectra for the $x=0.3$ crystal, (c) in-plane reflectivity spectra for the $x=0.4$ crystal, and (d) c-axis reflectivity spectra for the $x=0.4$ crystal.

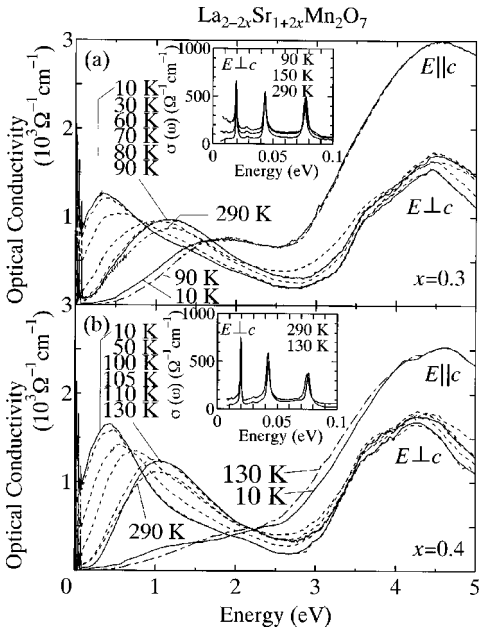

FIG. 5. Temperature dependence of in-plane ($E\perp c$) and c-axis ($E\|c$) optical conductivity spectra for $La_{2-2x}Sr_{1+2x}Mn_2O_7$ crystals of (a) $x=0.3$ and (b) $x=0.4$ with the 3D spin-ordering temperature $T_c\approx 90$ K ($x=0.3$) and 120 K ($x=0.4$), respectively. Solid lines represent the spectra at 10 K, 90 K ($x=0.3$), or 130 K ($x=0.4$). The insets to (a) and (b) are magnified spectra of in-plane low-energy optical conductivity at temperatures above T_c for $x=0.3$ and 0.4, respectively.

doped crystal[30] is also explained by the dominant x^2-y^2-orbital character as argued in the following section.

IV. TEMPERATURE DEPENDENCE OF OPTICAL SPECTRA FOR $x=0.3$ AND 0.4 WITH METALLIC GROUND STATE

In this section, we discuss the electronic structural change in the course of the transition from PI to a magnetically ordered metallic state for the $x=0.3$ ($T_c\approx 90$ K) and 0.4 ($T_c\approx 120$ K) crystals using the optical spectra on an energy scale of several eV. Both samples have a ferromagnetic bilayer unit at low T, while the adjacent bilayer units are ordered antiferromagnetically for $x=0.3$ and forromagnetically for $x=0.4$.

We show in Fig. 4 the T dependence of reflectivity spectra for the respective polarizations, $E\perp c$ and $E\|c$, and for the respective compositions, $x=0.3$ and 0.4, at the temperatures below T_c. Spiky structures in the far-infrared region ($\hbar\omega < 0.07$ eV) are due to optical phonon modes. The number of phonon modes is found to be consistent with the factor group analysis (six in-plane and five out-of-plane modes), although all the phonon modes are not clearly discerned in this figure. As T is decreased below T_c, the both $E\perp c$ spectra show a drastic change on a large energy scale up to 3 eV. By contrast, the $E\|c$ spectra show little change. Thus the $E\|c$ spectra behave like insulating ones over the whole T region in accord with their high resistivity value even in the FM phase [see Figs. 1(a) and (b)].

Figure 5 shows the T dependence of the optical conductivity spectra of (a) the $x=0.3$ and (b) 0.4 single crystals for $E\perp c$ and $E\|c$ which were deduced by Kramers-Kronig analysis of the reflectivity data. As T decreases from 290 K to just above T_c, the spectra remains almost unchanged for both $x=0.3$ and 0.4 except for the slight increase (decrease) of the low-energy spectral weight (see the inset to Fig. 5). Thus the optical conductivity spectra are consistent with the extremely bad metal (or insulating) behavior of the resistivity above T_c. Below T_c, a conspicuous T-dependent change for the in-plane ($E\perp c$) spectra is observed up to 3 eV, where the spectra are dominated by the intra- and interband transitions relevant to O $2p$- and Mn $3d$ e_g-like hybridized states as mentioned in the previous section. By contrast, the $E\|c$ spectra show a minimal T dependence, except for slight accumulation of the spectral weight below 1.5 eV with decreasing T below T_c. A difference in the interbilayer coupling least affects the optical conductivity spectra since the interbilayer exchange coupling along the c axis may be two orders of magnitude smaller than the intrabilayer one.[39]

With decreasing T below T_c a large spectral change occurs in the $E\perp c$ spectra over an energy range of 0-3 eV. Importantly, most of the transferred spectral weight does not form the Drude-like coherent peak centered at $\omega=0$ expected for the simple DE model, but makes a peak around 0.4 eV. This signals unconventional charge dynamics in the metallic state of these bilayered manganites. This low-energy feature is discussed in the following section using the magnified low-energy spectra (see the insets to Fig. 6). Here, let us first discuss the overall spectral-weight transfer as observed. To estimate the transferred spectral weight, we have calculated the $N_{\rm eff}(\omega)$ spectra, which was defined by Eq. (1). Figures 7(c) and (d) show the T dependence of $N_{\rm eff}$ at $\omega_c=0.8$ eV, a cutoff energy for the estimate of the transferred low-energy spectral weight. Between 290 K and T_c, $N_{\rm eff}(\omega_c)$ are nearly constant. Once the compound undergoes the 3D spin ordering transition, $N_{\rm eff}(\omega_c)$ shows a conspicu-

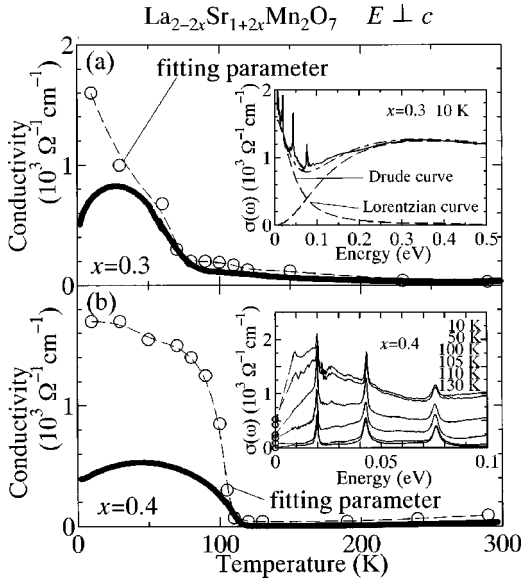

FIG. 6. Temperature dependence of the optically deduced $\omega \rightarrow 0$ conductivity as the fitting parameter (see text) compared with the dc conductivity data for (a) $x=0.3$ and (b) 0.4 crystals. Inset to (a): The 10-K in-plane optical conductivity spectra (solid lines) for the $x=0.3$ crystal with the fitting curve (dashed and dot-dashed lines). Inset to (b): The magnified optical conductivity spectra in the low-energy region below 0.1 eV as well as the dc conductivity data (open circles). Dashed lines in this inset are merely the guide to the eyes.

ous increase in accord with the occurrence of the metallic conduction.

Similar spectral change with the decrease of T or with evolution of the spontaneous magnetization was also observed for the underdoped pseudocubic perovskite manganite

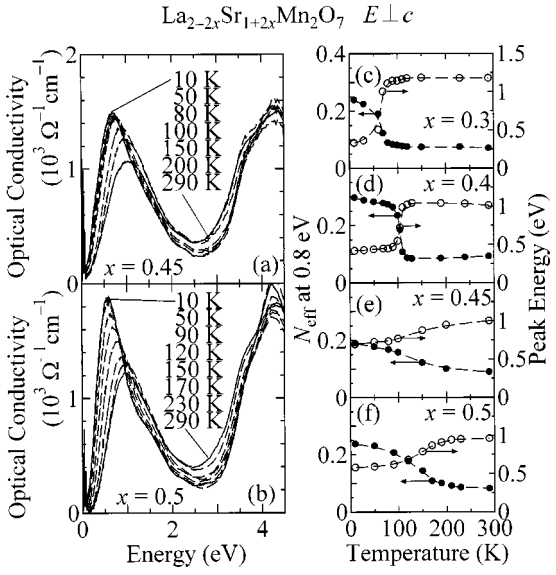

FIG. 7. Left panel: Temperature dependence of the in-plane optical conductivity spectra of $La_{2-2x}Sr_{1+2x}Mn_2O_7$ single crystals which show the A-type magnetic ordering in the ground state; (a) $x=0.45$ and (b) $x=0.5$. Solid lines represent 290 and 10 K spectra. Right panel: Temperature dependence of the effective number of electrons at 0.8 eV (closed circles) and the lowest-peak energy (see text; open circles) for (c) $x=0.3$, (d) 0.4, (e) 0.45, and (f) 0.5.

crystals.[8–12] Such a large spectral change as observed in perovskite manganites has been discussed in various contexts; (1) the T-dependent change of the density of states for the spin-polarized e_g-state conduction bands with a large exchange splitting exceeding the bandwidth,[8,16] (2) the JT polaron band with T-dependent effective coupling strength,[9–12,17] (3) the T-dependent change of the interband transitions between the different-orbital branches at nonspecific k points.[19,20] All the scenarios may be relevant to the observed features, perhaps depending on the energy region. For example, the spectral change extending up to as large an energy scale as 3 eV cannot be accounted for by (2) or (3), but should be interpreted in terms of the electronic-structural change on an energy scale of Hund's-rule coupling as in (1). Namely, the model considers the conduction band split by the Hund's-rule coupling energy ($\approx$2 eV), that is, in fact, demonstrated by the local spin density approximation band-structure calculation on this compound.[15,40] Above T_c, the lower-lying up-spin and down-spin bands are equally occupied, while in the ferromagnetic ground state with full spin polarization the partially occupied up-spin band and the totally unoccupied down-spin band are separated by the exchange splitting. The presently observed spectral weight transfer with onset of the magnetization can partly be assigned to the change in the character of the conduction-electron related transitions, namely, from the interband transition between the exchange-split conduction bands to the intraband excitation within the up-spin band, as in the case of $La_{1-x}Sr_xMnO_3$.[8]

The overall feature of the T-dependent change of the in-plane low-energy conductivity spectrum can thus be explained similarly to the case of the 3D analog, $La_{1-x}Sr_xMnO_3$, yet some distinct features can be noticed for this quasi-2D ferromagnet in addition to their anisotropic behavior. While the low-energy (<1 eV) spectral weight is rapidly accumulated with the decrease of T, the 1-eV peak shift towards the lower energy to form the broad peak around 0.4 eV at the lowest T. The formation of such a mid-infrared peak and the shift with T might imply the small-polaronic conduction in this system. According to a conventional small-polaron model,[41] the peak energy of the $\sigma(\omega)$ corresponds approximately to twice the polaron binding energy. In fact, the 290 K (or higher-T) in-plane spectrum for the $x=0.4$ can be fit with a set of polaron parameters (e.g., binding energy $E_b=0.535$ eV and hopping energy $J=0.59$ eV). However, such a calculation fails to reproduce the shape of the lower-T $\sigma(\omega)$ spectrum that shows a subsisting low-energy (down to $\omega=0$ eV) tail as well as a pronounced peak structure around 0.4 eV. As a more suitable model, we may consider the dynamical mean-field calculation (infinite-dimensional approach) on the dynamic JT effect [the above scenario (2)] by Millis *et al.* (see Ref. 17). In fact, the calculated JT polaron spectra[17] with the electron-phonon coupling strength $\lambda \approx 1.08$ can qualitatively reproduce the observed T-dependent feature that the 1-eV peak around and above T_c is gradually shifted to a lower energy (down to 0.4 eV) with increasing spectral weight. (In this calculation, J_H is assumed infinite, so that the spectral feature with higher-energy than the JT coupling energy cannot be discussed.) The peak shift is assigned to the decrease of the effective electron-phonon coupling due to the increase of the kinetic energy. To be more quantitative about the singu-

lar shape of the $\sigma(\omega)$ observed in the *metallic* ground state, however, the consideration of the collective nature of the dynamic JT distortion or the short-range orbital ordering would be necessary for this quasi-2D system beyond the infinite-dimensional approach.

V. INCOHERENT CHARGE DYNAMICS IN THE LOW-ENERGY REGION

Let us discuss in this section the low-energy electronic structure which manifests itself in the in-plane spectrum of the barely metallic compounds. Since the zero-energy extrapolation of the optical conductivity spectra should coincide with the dc conductivity value, the lowest energy spectral shape is important from the view point of the metal-insulator transition. As seen in the magnified optical conductivity spectrum [the inset to Fig. 6(a)], the spectrum may consist of two parts, a coherent part (which bears quite a small spectral weight) and an incoherent part dominated by the 0.4-eV peak. For the quantitative analysis, we adopt a conventional Drude (coherent) and Lorentz (incoherent) curve fitting procedure to separate the spectrum into the respective components. We used following formula ($i=1$ in this case):

$$\sigma(\omega)=\frac{\sigma_0}{1+(\omega\tau)^2}+\sum_i \frac{S\omega_0^2\gamma\omega^2}{(\omega_0^2-\omega^2)^2+\gamma^2\omega^2}. \qquad (2)$$

Here, σ_0 represents the dc ($\omega\rightarrow 0$) conductivity, and τ and $1/\gamma$ represent relaxation time. ω_0 and S are resonance frequency and oscillator strength, respectively. The inset to Fig. 6(a) exemplifies the comparison of the fitting curves with the experimental data ($x=0.3$) at 10 K. In this energy region, we have a good agreement between fitting and experimental curves for each composition, except for the very low-energy region below 0.03 eV (due to the localization effect as mentioned below). The agreement assures the adequacy of this procedure. Thus we could roughly decompose the Drude part and calculate the Drude weight $m\sigma_0/Ne^2\tau$ (DW). The DW is proportional to the ratio of carrier number to effective mass in the case of a conventional metal. The calculated DW at the lowest temperature (10 K) are 0.03 ($x=0.3$) and 0.035 ($x=0.4$). These small values mean that the effective masses are ten times heavier than free electron one, given that the carrier density per Mn is equal to the nominal hole doping x. This is consistent with the ''ghost'' Fermi surface or ''soft-gap'' feature observed in the photoemmission spectra.[15] Such a small DW has been also observed for the pseudocubic manganites,[8] while the interpretation by the enhanced carrier mass is not consistent with the magnitude of electron specific heat which shows the least mass renormalization effect.[42]

We show in Fig. 6 the T dependence of the fitting parameter σ_0 ($\omega\rightarrow 0$ optical conductivity) with comparison of dc conductivity values (σ_{dc}) by a conventional four-probe measurement. The T dependence of σ_0 and σ_{dc} is nearly parallel around T_c, but not below 40 K. In the low-T region below 40 K, the σ_0 value monotonously increases, whereas σ_{dc} decreases with decreasing T. The inset to Fig. 6(b) shows this situation more clearly. The optical conductivity spectra magnified in the low-energy (0-0.1 eV) region in comparison with the measured dc conductivity below T_c are shown in the figure. The zero-frequency extrapolation of the optical conductivity are apparently higher than the σ_{dc} values. The Drude-like increase of $\sigma(\omega)$ is barely observed below 0.05 eV, but $\sigma(\omega)$ seems to fall again below 0.02 eV towards the σ_{dc} value. In other words, low-energy spectra are not consistent with a Drude model below 40 K. Recent measurements of low-T (down to 30 mK) resistivity in the bilayered compounds show that the resistivity is proportional to $\sqrt{T}$ and remains finite at the lowest T, implying 3D localization behavior.[42] Thus in the present quasimetallic layered manganites ($x=0.3$ and 0.4) the diffuse carrier motion even in the fully spin-polarized ground state is governed by two energy scales: One is due to the presence of 0.3–0.4 eV incoherent band that is ascribed to the dynamical lattice distortion and relatively reduces the DW. The other is the suppression of the Drude peak below 0.02 eV (see the inset to the lower panel of Fig. 6). The latter localization effect perhaps arises from the quasi-2D electronic structure and/or the inherent charge/orbital density wave instability (see the discussion in Sec. VII).

VI. TEMPERATURE DEPENDENCE OF THE OPTICAL SPECTRA IN CANTED ANTIFERROMAGNETIC OR *A*-TYPE ANTIFERROMAGNETIC NONMETALLIC PHASE

We show in Figs. 7(a) and (b) the T dependence of the in-plane optical conductivity spectra for the $x=0.45$ and 0.5 crystals, respectively, which show *A*-type AF (or canted antiferromagnetic) nonmetallic phase in a low-T region. The lowest-T (10 K) spectral shape of each compound rather resembles that of the FM phase in this energy range except for the slight difference of peak position (higher for $x=0.45$ and 0.5) and the existence of the clear gap. The gap feature is consistent with the observed high resistivity. To compare the *A*-type AF case with the FM one in the light of the T dependent spectral change, we show in Figs. 7(c)–(f) the T dependence of the $N_{\rm eff}$ at 0.8 eV, which measures the low-energy transferred spectral weight, and the energy of the lowest peak ($\sim$ 1 eV at 290 K) of the optical conductivity spectrum for each composition. In the nonmetallic compounds ($x=0.45$ and 0.5), the magnitude of the transfered spectral weight and also the shift of the peak energy with T is as large as that of the FM case, yet the T dependence of each value is distinctly different. For the FM case, the spectral change is very sharp and limited in a narrow T region near below T_c, while more gradual for the *A*-type AF case below $T_c\approx 200$ K. However, this tendency is consistent with the different T dependence of the order parameter for the magnetic ordering.[30,43,44] In other words, the large spectral weight transfer for these nonmetallic compounds are also due to the ferromagnetic ordering in each MnO_2 monolayer.

In the case of *A*-type AF phase there is a clear gap feature and no Drude-like response even at the lowest T (10 K). The difference between the *A*-type AF phase and the FM phase is only the spin direction, i.e., antiparallel or parallel, between each MnO_2 single plane within a bilayer unit, and such difference cannot explain the difference of $\sigma(\omega)$ between AF and FM phase. The AF coupling between the MnO_2 plane restricts the carrier motion within each plane. This sup-

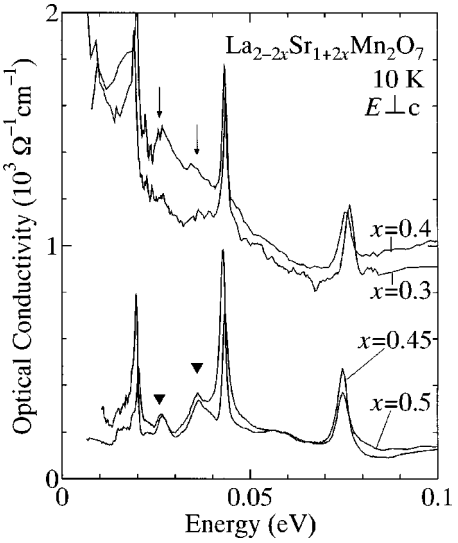

FIG. 8. The doping dependence of the magnified in-plane optical conductivity spectra at 10 K. Triangles indicate the activated modes for $x=0.45$ and 0.5, and arrows the traces of these modes for $x=0.4$ (see text).

presses the splitting of the in-plane band dispersion arising from the $3z^2-r^2$ orbital-mediated interplane interaction, and hence may enhance the electronic or lattice instability due to the 2D nature. A mean-field calculation which assumes the orbital ordered structure suggests the *metallic A*-type AF phase with the ordering of the x^2-y^2 orbitals in such a high-doping region. On the other hand, according to the exact diagonalization calculation based on the 2D orbital *t-J* model,[45] the x^2-y^2 orbital ordering as well as the pseudogap structure appears as a consequence of the orbital correlation. However, both theories suggest the existence of large Drude (or low-energy spectral) weight, which is in contradiction with the present experimental result. Concerning this contradiction, we argue a possible effect of short-range charge ordering, and the present spectroscopic evidence for it in the next section.

VII. IMPLICATION OF SHORT-RANGE CHARGE ORDERING IN OPTICAL-PHONON SPECTRA

Figure 8 shows the optical phonon spectra for the respective crystals at 10 K, i.e., in the spin-ordered phase (FM or *A*-type AF). As clearly seen, the number of observed phonon modes is different depending on the doping level x or the magnetic structure. The *A*-type AF phase ($x=0.45$ and 0.5) spectra show at least six modes, while the FM phase ($x=0.3$ and 0.4) spectra show only three modes. In the *A*-type AF phase additional modes are observed around 0.028 and 0.038 eV (indicated by triangles), which are rather broad in shape compared with other modes and hardly discernible in the FM phase spectra. The T dependence of these modes are peculiar. We show the T dependence of the in-plane optical phonon spectrum for the $x=0.5$ crystal in Fig. 9(a). With decreasing T below about 200 K the above-mentioned two modes, named (i) and (ii), gradually grow in intensity, in accord with onset of the *A*-type magnetic ordering and the electronic structural change (see Ref. 43 and the previous section). To evaluate the oscillator strength of these modes,

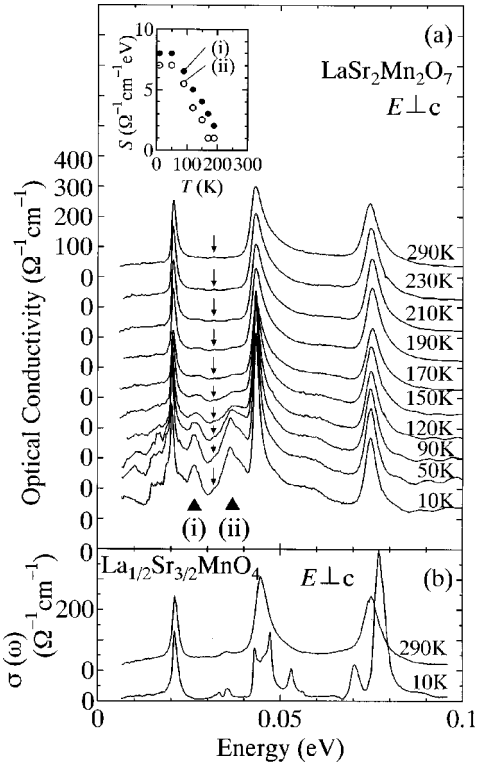

FIG. 9. Temperature dependence of the optical-phonon mode spectra for the layered (Ruddlesden-Popper series) compounds with $x=0.5$. (a) The in-plane spectrum for $La_{2-2x}Sr_{1+2x}Mn_2O_7$ ($x=0.5$). Arrows and triangles indicate the original and activated modes, respectively (see the text). (b) The in-plane spectrum for $La_{1-x}Sr_{1+x}MnO_4$ ($x=0.5$) which shows charge-orbital ordering transition at about 210 K. Inset to (a): Temperature dependence of the oscillator strength of the activated phonon modes (i) and (ii).

we adopt the aforementioned Lorentz curve fitting procedure [Eq. (2)]. The results are shown in the inset to Fig. 9(a). The oscillator strengths of these modes gradually increase in a parallel manner with decreasing T, as if it were correlated to the evolution of the *A*-type magnetic ordering.[43]

Factor group analysis tells us the existence of six infrared-active in-plane optical phonon modes for the simple bilayer manganites with D_{4h} symmetry. For the single-layered compound [Fig. 9(b)], distinct four phonon peaks are observed in the 290-K spectrum and this spectral shape is similar to the shape of the bilayered one in the paramagnetic phase, in which four peaks, 0.02, 0.032, 0.04, and 0.075 eV, are also observed. This means that these phonon modes in the paramagnetic phase have the common origin. In addition, these four modes are also observed in the *A*-type AF phase, though the 0.032-eV peak (indicated by arrows) may be difficult to be separated by the other peak structures because of its quite small spectral weight. In contrast, the modes (i), (ii), and also the broad peak around 0.06 eV are absent in the 290-K spectrum of the single-layered compound. Then, two possibilities are to be considered in the present T-dependent oscillator strength change, (a) enhancement of the intensity of the original phonon modes which exist already but are too weak to be discernible above T_N, (b) appearance of newly activated modes or splitting of original modes due to the lowering of the symmetry. The present case is likely interpreted by the latter scenario because of distinct change in the observ-

able mode number. In addition, the broadened feature of the relevant modes may suggest presence of fluctuation or spatial inhomogeneity of local lattice distortion. One of the candidates for such a lattice distortion might be a CE-type charge ordering (CO) phenomenon since a recent neutron-scattering study shows the coexistence of the CE-type CO and *A*-type AF phase in the low-T region.[43] However, judging from the pattern of the phonon spectra for the single-layered crystal $La_{1/2}Sr_{3/2}MnO_4$ in the CE-type charge ordering (CO) phase [see the 10-K spectrum in Fig. 9(b)], these activated modes are not characteristic at all of the CE-type CO phase. For example, the 0.07-eV mode, that is hallmark of the CE-type CO state, does not show up in the spectrum for the bilayered compound.[46] Thus the origin of the (i) and (ii) modes should be the lattice distortion accompanied by the *A*-type spin ordering. By now, the *A*-type ordering of the manganites in the higher doping region has been attributed to the x^2-y^2 type orbital ordering (OO).[47,48] This OO pattern itself, even accompanied by coherent JT distortion, is consistent with the original K_2NiF_4-type structure of this system and may not need to further lower the lattice symmetry nor to increase the phonon number. Therefore we have to seek another mechanism for the origin of lattice distortion.

A plausible lattice distortion accompanied by the *A*-type spin-ordered and x^2-y^2 type orbital-ordered state is the alternate breathing-type lattice deformation. Such a lattice structural change has not been confirmed experimentally as yet for the pseudocubic manganite, but been suggested by unrestricted Hartree-Fock calculations on the multiband *p-d* model.[49] According to the above calculation, the *A*-type AF state is stabilized by the (π,π) ordering of the breathing-type distortion within the MnO_2 plane, that is the ordering of Mn^{3+} ion with an electron in x^2-y^2 orbital and Mn^{4+} ion.

Such a two-dimensional metallic state as the *A*-type state is amenable to the electron-lattice coupled instability, e.g., the charge-density-wave instability. The (π,π) charge-density modulation as suggested by the calculations[45,49] and its coupling to the breathing-type lattice modulation is likely responsible for the observed phonon-spectral anomaly. This may also give rise to a plausible mechanism that prevents the coherent carrier motion and produces the pseudogap structure in the *A*-type phase as observed. It is noted in Fig. 8 that a trace of the activated modes is barely discernible even for the $x=0.4$ spectrum (indicated by arrows) at the nearly identical energy positions. This may signal that such an electron-lattice coupling also plays an important role in producing the 0.4-eV peak of the in-plane spectra for $x=0.3$ and 0.4 crystals even in the FM phase, although the value of reflectivity is too high to assure the existence of the activated-phonon structure from the reflectivity or transformed conductivity spectra.

VIII. SUMMARY

We have measured the reflectivity spectra of the bilayered manganites $La_{2-2x}Sr_{1+2x}Mn_2O_7$ $(0.3\leqslant x\leqslant 0.5)$ and deduced the optical conductivity spectra. The change in the out-of-plane polarized spectra indicates that hole doping gradually changes the e_g electron orbital character from $3z^2-r^2$ to x^2-y^2 like. In the course of the thermally induced PI to FM transition, the in-plane electronic structure as probed by the optical conductivity spectra shows drastic change on a large energy scale due to the various mechanisms depending on the respective energy regions with lowering temperature, the spectral weight is accumulated in a low-energy region (<0.8 eV) for the FM compounds ($x=0.3$ and 0.4), while the conductivity spectrum still show a broad peak profile around 0.4 eV. Thus the FM ground-state spectrum shows an extremely incoherent nature down to zero energy with extremely small Drude weight. In a further lower energy region (<0.02 eV), the effect of the localization is clearly seen as the steep decrease of the optical conductivity toward the low dc conductivity. Even in the *A*-type antiferromagnetic nonmetallic phase, low-energy transferred spectral weight is as large as in the FM phase. In connection with its gap feature, we found the spectroscopic evidence for the different lattice distortion which strongly correlates with the *A*-type magnetic or (x^2-y^2)-type orbital order and suggests a different type of concomitant charge- and orbital-ordered state.

ACKNOWLEDGMENTS

We thank Y. Moritomo and K. Ookura for their collaboration at the early stage of this study, and T. Saitoh, D. S. Dessau, Y. Okimoto, K. Yamamoto, E. Saitoh, A. Fujimori, and M. Kubota for fruitful discussions. One of the authors (T.I.) was supported from the Japan Society for the Promotion of Science for Japanese Junior Scientists. This work was supported by the Grant-In Aids for Scientific Research from the Ministry of Education, Science, Culture and Sport, Japan also by the NEDO.

*Present address: Department of Condensed Matter Physics, Tokyo Institute of Technology, Oh-okayama, Tokyo 152-8551, Japan.

†Present address: Department of Applied Physics, University of Tokyo, Tokyo 113-8656, Japan.

‡Present address: Graduate School of Frontier Sciences, University of Tokyo, Tokyo 113-8656, Japan.

[1] R. von Helmolt, J. Wecker, B. Holzapfel, L. Schultz, and K. Samwer, Phys. Rev. Lett. **71**, 2331 (1993).

[2] S. Jin, T.H. Tiefel, M. McCormack, R.A. Fastnacht, R. Ramesh, and L.H. Chen, Science **264**, 413 (1994).

[3] K. Chahara, T. Ohno, M. Kasai, and Y. Kozono, Appl. Phys. Lett. **63**, 1990 (1993).

[4] Y. Tokura, A. Urushibara, Y. Moritomo, T. Arima, A. Asamitsu, G. Kido, and N. Furukawa, J. Phys. Soc. Jpn. **63**, 3931 (1994); A. Urushibara, Y. Moritomo, T. Arima, A. Asamitsu, G. Kido, and Y. Tokura, Phys. Rev. B **51**, 14 103 (1995).

[5] C. Zener, Phys. Rev. **82**, 403 (1951).

[6] P.W. Anderson and H. Hasegawa, Phys. Rev. **100**, 675 (1955).

[7] P.-G. de Gennes, Phys. Rev. **118**, 141 (1960).

[8] Y. Okimoto, T. Katsufuji, T. Ishikawa, T. Arima, and Y. Tokura, Phys. Rev. B **55**, 4206 (1997).

[9] K.H. Kim, J.H. Jung, and T.W. Noh, Phys. Rev. Lett. **81**, 1517 (1998).

[10] K.H. Kim, J.H. Jung, D.J. Eom, T.W. Noh, Jaejun Yu, and E.J. Choi, Phys. Rev. Lett. **81**, 4983 (1998).

[11] S.G. Kaplan, M. Quijada, H.D. Drew, D.B. Tanner, G.C. Xiong, R. Ramesh, C. Kwon, and T. Venkatesan, Phys. Rev. Lett. **77**, 2081 (1996).

[12] M. Quijada, J. Cerne, J.R. Simpson, H.D. Drew, K.H. Ahn, A.J. Millis, R. Shreekala, R. Ramesh, M. Rajeswari, and T. Venkatesan, Phys. Rev. B **58**, 16 093 (1998).
[13] Y. Moritomo, A. Machida, K. Matsuda, M. Ichida, and A. Nakamura, Phys. Rev. B **56**, 5088 (1997).
[14] T. Saitoh, A. Sekiyama, K. Kobayashi, T. Mizokawa, A. Fujimori, D.D. Sarma, Y. Takeda, and M. Takano, Phys. Rev. B **56**, 8836 (1997).
[15] D.S. Dessau, T. Saitoh, C.-H. Park, Z.-X. Shen, P. Villella, N. Hamada, Y. Moritomo, and Y. Tokura, Phys. Rev. Lett. **81**, 192 (1998).
[16] N. Furukawa, J. Phys. Soc. Jpn. **64**, 3164 (1995).
[17] A.J. Millis, R. Mueller, and B.I. Shraiman, Phys. Rev. B **54**, 5405 (1996).
[18] S. Yunoki, A. Moreo, and E. Dagotto, Phys. Rev. Lett. **81**, 5612 (1998).
[19] H. Shiba, R. Shiina, and A. Takahashi, J. Phys. Soc. Jpn. **66**, 941 (1997).
[20] P.E. de Brito and H. Shiba, Phys. Rev. B **57**, 1539 (1998).
[21] A.S. Alexandrov and A.M. Bratkovsky, Phys. Rev. B **60**, 6215 (1999).
[22] Y. Moritomo, A. Asamitsu, H. Kuwahara, and Y. Tokura, Nature (London) **380**, 141 (1996).
[23] T. Kimura, Y. Tomioka, H. Kuwahara, A. Asamitsu, M. Tamura and Y. Tokura, Science **274**, 1698 (1996).
[24] R. Osborn, S. Rosenkranz, D.N. Argyriou, L. Vasiliu-Doloc, J.W. Lynn, S.K. Sinha, J.F. Mitchell, K.E. Gray, and S.D. Bader, Phys. Rev. Lett. **81**, 3964 (1998).
[25] T. Ishikawa, T. Kimura, T. Katsufuji, and Y. Tokura, Phys. Rev. B **57**, R8079 (1998).
[26] D.N. Argyriou, J.F. Mitchell, J.B. Goodenough, O. Chmaissem, S. Short, and J.D. Jorgensen, Phys. Rev. Lett. **78**, 1568 (1997).
[27] J.F. Mitchell, D.N. Argyriou, J.D. Jorgensen, D.G. Hinks, C.D. Potter, and S.D. Bader, Phys. Rev. B **55**, 63 (1997).
[28] T. Kimura, A. Asamitsu, Y. Tomioka, and Y. Tokura, Phys. Rev. Lett. **79**, 3720 (1997).
[29] T.G. Perring, G. Aeppli, T. Kimura, Y. Tokura, and M.A. Adams, Phys. Rev. B **58**, R14 693 (1998).
[30] K. Hirota, Y. Moritomo, H. Fujioka, M. Kubota, H. Yoshizawa, and Y. Endoh, J. Phys. Soc. Jpn. **67**, 3380 (1998).
[31] T. Kimura, R. Kumai, Y. Tokura, J.Q. Li, and Y. Matsui, Phys. Rev. B **58**, 11 081 (1998).
[32] T. Arima, Y. Tokura, and J.B. Torrance, Phys. Rev. B **48**, 17 006 (1993).
[33] Y. Moritomo, T. Arima, and Y. Tokura, J. Phys. Soc. Jpn. **64**, 4117 (1995).
[34] T. Ishikawa, K. Ookura, and Y. Tokura, Phys. Rev. B **59**, 8367 (1999); In this CO system, the 1-eV peak moves towards higher energy up to about 1.4 eV in accord with the development of the CO order parameter.
[35] J.H. Jung, J.S. Ahn, Jaejun Yu, T.W. Noh, and Jinhyoung Lee Phys. Rev. B **61**, 6902 (2000).
[36] In the recent optical study (Ref. 50), this 1-eV peak was assigned to the intersite *d-d* transition between JT split Mn^{3+} e_g orbital and nearest-neighbor degenerated Mn^{4+} e_g orbital. However, such a simple and one-particle picture considering the JT interaction alone may be insufficient, at least for the present system from the following point of view on the energy scale (Ref. 53). In the bilayer system, there is static and coherent distortion of MnO_6 octahedra (2% change in the equatorial and apical Mn-O bond lengths) (Refs. 27 and 37), and hence the e_g level already splits uniformly. Such a static e_g-level splitting energy (E_0) for the $x=0.4$ crystal is about 0.4 eV from the x-ray absorption data (Ref. 51), which means that JT polaron binding energy (E_{JT}) is $E_0/4=0.1$ eV (Ref. 52). In addition, since there are two linked Mn sites along the *c* axis in the bilayer unit, there would exist the remnant of the in-plane 1-eV peak also in the *c*-axis spectra, if the local JT scenario were correct.
[37] T. Kimura, Y. Tomioka, A. Asamitsu, and Y. Tokura, Phys. Rev. Lett. **81**, 5920 (1998).
[38] M. Medarde, J.F. Mitchell, J.E. Millburn, S. Short, and J.D. Jorgensen, Phys. Rev. Lett. **83**, 1223 (1999).
[39] T. Chatterji, L.P. Regnault, P. Thalmeier, R. Suryanarayanan, G. Dhalenne, and A. Revcolevschi, Phys. Rev. B **60**, R6965 (1999).
[40] N. Hamada *et al.* (unpublished).
[41] M.I. Klinger, Phys. Solid State **11**, 499 (1965); **12**, 765 (1965); H.G. Reik and D. Hesse, J. Phys. Chem. Solids **28**, 581 (1967).
[42] T. Okuda, T. Kimura, and Y. Tokura, Phys. Rev. B **60**, 3370 (1999).
[43] M. Kubota, H. Yoshizawa, Y. Moritomo, H. Fujioka, K. Hirota, and Y. Endoh, J. Phys. Soc. Jpn. **68**, 2202 (1999).
[44] As for the $x=0.5$ crystal, the CO phase exists at least in the intermediate *T* region between 210 and 60 K (Refs. 31 and 43), but there is no clear spectral change related to the CO phase, in contrast to the case of $La_{1/2}Sr_{3/2}MnO_4$ (nominal hole concentration $x=0.5$) crystal (see the previous section) where a large energy-scale spectral change relating to the CO transition has been observed. The optical-phonon mode spectra, which are very sensitive to the CO related lattice distortion as mentioned in Sec. VII, could not detect obvious CO signal (see Fig. 9) for the bilayer $x=0.5$ crystal. Thus the CO phase in the present bilayered manganite should have a much smaller amplitude of the charge/orbital modulation than in the single-layered one.
[45] F. Mack and P. Horsh, Phys. Rev. Lett. **82**, 3160 (1999).
[46] The CO phase can be easily stabilized by strain in manganite. Actually, the phonon spectra of a polished (and hence perhaps stressed) surface showed clearly the splitting of the stretching mode (≈ 0.07 eV) which signals the occurrence of the CO state. At that time, the 0.027- and 0.038-eV modes were simultaneously observed without obvious enhancement or suppression perhaps due to the phase separation.
[47] R. Maezono, S. Ishihara, and N. Nagaosa, Phys. Rev. B **58**, 11 583 (1998).
[48] H. Kawano, R. Kajimoto, H. Yoshizawa, Y. Tomioka, H. Kuwahara, and Y. Tokura, Phys. Rev. Lett. **78**, 4253 (1997).
[49] T. Mizokawa and A. Fujimori, Phys. Rev. B **56**, R493 (1997).
[50] J.H. Jung, K.H. Kim, T.W. Noh, E.J. Choi, and Jaejun Yu, Phys. Rev. B **57**, R11 043 (1998).
[51] J.-H. Park, T. Kimura, and Y. Tokura, Phys. Rev. B **58**, R13 330 (1998).
[52] A.J. Millis, Phys. Rev. B **53**, 8434 (1996).
[53] Dynamical JT distortion, which would not show up in the average lattice parameters, might be relevant to the formation of the JT polaron with such a large binding energy. Then the local JT distortion should be as large as 10% of the difference of the relevant two Mn-O bond lengths. A recent study of pulsed neutron diffraction by D. Louca, T. Egami, E.L. Brosha, H. Röder, and A.R. Bishop [Phys. Rev. B **56**, R8475 (1997)] has evidenced such a large ($\sim 10\%$) local distortion of octahedron in pseudocubic $La_{1-x}Sr_xMnO_3$ system ($0 \leqslant x \leqslant 0.4$). Conversely, such a large local distortion should cause the strong spatial correlation, as argued in the text.